Published in final edited form as:
Biochemistry. 2007 May 8; 46(18): 5293–5304. doi:10.1021/bi700065h.

Purification and Characterization of the Fe^{II}- and α-Ketoglutarate-Dependent Xanthine Hydroxylase from *Aspergillus nidulans*†

Gabriela M. Montero-Morán[‡,§], **Meng Li**[‡,‖], **Erika Rendòn-Huerta**[⊥], **Fabrice Jourdan**[¶], **David J. Lowe**[¶], **Andrew W. Stumpff-Kane**[#], **Michael Feig**[‖,#], **Claudio Scazzocchio**[§,+], and **Robert P. Hausinger**[#,○,*]

§*Institut de Génétique et de Microbiologie, Université Paris-Sud, Bâtiment 409, UMR 8621 CNRS, 91405 Orsay Cedex, France*

‖*Department of Chemistry, Michigan State University, East Lansing, Michigan 48824-1322, USA*

⊥*Departamento de Bioquimica, Facultad de Medicina, Universidad Nacional Autonoma de Mexico, Mexico City, DF, Mexico*

¶*Department of Biological Chemistry, John Innes Centre, Colney Lane, Norwich NR4 7UH, U.K.*

#*Department of Biochemistry and Molecular Biology, Michigan State University, East Lansing, MI 48824-1319*

+*Institut Universitaire de France*

○*Department of Microbiology and Molecular, Michigan State University, East Lansing, Michigan 48824-4320, USA*

Abstract

His_6-tagged xanthine/α-ketoglutarate (αKG) dioxygenase (XanA) of *Aspergillus nidulans* was purified from both the fungal mycelium and recombinant *Escherichia coli* cells, and the properties of the two forms of the protein were compared. Evidence was obtained for both *N*- and *O*-linked glycosylation on the fungus-derived XanA, which aggregates into an apparent dodecamer, while bacteria-derived XanA is free of glycosylation and behaves as a monomer. Immunological methods identify phosphothreonine in both forms of XanA, with phosphoserine also detected in the bacteria-derived protein. Mass spectrometric analysis confirms glycosylation and phosphorylation of the fungus-derived sample, which also undergoes extensive truncation at its amino terminus. Despite the major differences in properties of these proteins, their kinetic parameters are similar (k_{cat} 30-70 s^{-1}, K_m of αKG 31-50 μM, K_m of xanthine ~45 μM, and pH optima at 7.0 to 7.4). The enzyme exhibits no significant isotope effect when using 8-^{2}H-xanthine; however, it demonstrates a two-fold solvent deuterium isotope effect. Cu^{II} and Zn^{II} potently inhibit the Fe^{II}-specific enzyme, whereas Co^{II}, Mn^{II}, and Ni^{II} are weaker inhibitors. NaCl decreases the k_{cat} and increases the K_m of both αKG and xanthine. The αKG cosubstrate can be substituted by α-ketoadipate (9-fold decrease in k_{cat} and 5-fold increase in the K_m compared to the normal α-keto acid), while the αKG analogue *N*-oxalylglycine is a competitive inhibitor (K_i 0.12 μM). No alternative purines effectively substitute for xanthine as a substrate, and only one purine analogue (6,8-dihydroxypurine) results in significant inhibition. Quenching of the endogenous fluorescence of the two enzyme forms by xanthine, αKG, and DHP

†These studies were supported by the National Institutes of Health (GM063584 to R.P.H.), NSF CAREER grant 0447799 (to M.F.), Université Paris-Sud (including a Post-doctoral Fellowship to G.M.-M.), CNRS and the Institut Universitaire de France (to C.S.), and EU Contract HPRN-CT-1999-084 (XONET to D.J.L and C.S.).

*To whom correspondence should be addressed: Department of Microbiology and Molecular Genetics, 6193 Biomedical Physical Sciences; Tel.: 517-355-6463 ext. 1610; Fax: 517-353-8957; E-mail:hausinge@msu.edu
‡These authors contributed equally to this work

was used to characterize their binding properties. A XanA homology model was generated on the basis of the structure of the related enzyme TauD (PDB code 1OS7) and provided insights into the sites of posttranslational modification and substrate binding. These studies represent the first biochemical characterization of purified xanthine/αKG dioxygenase.

Most organisms that metabolize xanthine possess a molybdopterin cofactor (Moco)[1]-containing enzyme that hydroxylates the substrate to form uric acid while transferring electrons to NAD (xanthine dehydrogenase) or oxygen (xanthine oxidase) (1). These enzymes, referred to here as xanthine hydroxylases, are conserved throughout living organisms, including archaea, bacteria, fungi, plants, and metazoans.

In 2005, a novel mechanism for xanthine metabolism was discovered in certain fungi (2). This finding arose out of the observation that all mutants of *Aspergillus nidulans* defective in xanthine dehydrogenase (i.e., with mutations affecting the structural gene *hxA*, the *cnx* genes for Moco synthesis, or *hxB* for sulfuration of Moco) retained the ability to grow on xanthine as sole nitrogen source (2,3). A mutation affecting this alternative process was identified, and the cognate gene *xanA* was localized to chromosome VIII (4). Subsequently, the *xanA* gene and its homologues from *Schizosaccharomyces pombe* and *Neurospora crassa* were cloned and further homologues were identified in several other fungi (but not outside the fungal kingdom). The *xanA* gene of *A. nidulans* is transcriptionally co-regulated with all other genes of the purine utilization pathway, including *hxA*, with its transcription depending on the same DNA binding factors, and this provides further evidence that its physiological role is xanthine oxidation (5). The XanA sequence shows some similarity with the taurine/α-ketoglutarate (αKG) dioxygenase (TauD) group of Fe^{II}- and αKG-dependent dioxygenases (2), including a clear conservation of the Fe^{II}- and αKG-binding sites. This homology suggested that the alternative xanthine oxidation mechanism present in some fungi might utilize an Fe^{II}-dependent xanthine/αKG dioxygenase. Such activity was demonstrated in both crude and partially purified extracts of fungal mycelia of strains that expressed the *xanA* gene (2). On the basis of the previously described mechanism for Fe^{II}/αKG hydroxylases (6), XanA is proposed to catalyze the series of reactions (αKG binding, xanthine binding, O_2 binding, αKG

[1]Abbreviations:

αKG α-ketoglutarate

DHP dihydroxypurine

Moco molybdopterin cofactor

NOG *N*-oxalylglycine

NTA nitrilotriacetic acid

PIXE particle induced X-ray emission

PNGase F *N*-glycosidase F

SDS-PAGE sodium dodecyl sulfate-polyacrylamide gel electrophoresis

TauD taurine/αKG dioxygenase.

decomposition and O-O cleavage to yield an Fe^{IV}-oxo species, hydrogen atom abstraction, and hydroxyl radical rebound) depicted in Scheme 1.

The wide range of Fe^{II}/αKG hydroxylases utilize a diverse array of primary substrates (reviewed in (6)); however, XanA is the first described enzyme of this group to hydroxylate a free purine base. In the fungal kingdom, this enzyme coexists with the classical xanthine hydroxylase; i.e., some fungi possess both xanthine hydroxylase and xanthine/αKG dioxygenase, while others possess only one or the other. Notably, yeasts as evolutionarily distant as *S. pombe* and *Kluveromyces lactis* are able to metabolize xanthine through the activity of a XanA homologue (2). They lack a classical xanthine dehydrogenase, and they are incapable of synthesizing Moco, which is universally present in the classical xanthine hydroxylases. The discovery of the novel Fe^{II}/αKG-dependent XanA enzyme poses both evolutionary and mechanistic problems. Is the xanthine-binding site of the newly identified enzyme at all similar to that of the classical xanthine hydroxylases (7,8) or to the recently described xanthine transporters (9,10)? Is the mechanism of hydroxylation similar to that described for TauD (11,12)? What are the evolutionary advantages and disadvantages of possessing the Moco-containing and Fe^{II}/αKG-dependent enzymes?

As a first step towards answering the above questions, we have purified His_6-tagged versions of XanA from its natural host, *A. nidulans*, and from *Escherichia coli*. We show that the protein differs in quaternary structure and in the identity of posttranslational modifications depending on whether it is derived from the fungal or bacterial host. In addition, we demonstrate that the fungus-derived protein is truncated at its amino terminus. We confirm that the enzyme is an Fe^{II}/αKG dioxygenase and show that the two forms of the protein exhibit similar pH dependence and kinetic parameters. We show that the enzyme exhibits a solvent isotope effect, but not a substrate isotope effect. In addition, we define the effects of different divalent metal ions, salt, and several αKG and xanthine analogues, including identification of alternate substrates and inhibitors. We use the endogenous fluorescence of the enzyme to monitor binding of αKG, xanthine, and a purine inhibitor, and deduce their dissociation constants. Finally, we generate a homology model of XanA and use it to provide insights into the likely sites of posttranslational modification and substrate binding. These studies present the first biochemical analyses of purified Fe^{II}-dependent xanthine/αKG dioxygenase.

EXPERIMENTAL PROCEDURES

Cloning for Overproduction of His_6-Tagged XanA in A. nidulans *and* E. coli, *Growth of Mycelia and Bacterial Cells, and Purification of XanA from each Source*

The details of these procedures are provided in Supporting Information. Enzyme samples were stored in buffer containing EDTA and/or imidazole to ensure the presence of apoprotein; these conditions minimize the aberrant metal-dependent side reactions known to damage other related enzymes (13-16).

Protein Analytical Methods

Routine determinations of protein concentration were carried out by the method of Bradford (17) with bovine serum albumin used as the standard. Qualitative measurement of protein overexpression and assessment of protein purity made use of sodium dodecyl sulfate polyacrylamide gel electrophoresis (SDS-PAGE) (18), with stacking and running gels containing 5 % and 12 % acrylamide. Standard proteins used for comparison included phosphorylase b, M_r 97,400; bovine serum albumin, M_r 66,200; ovalbumin, M_r 45,000; carbonic anhydrase, M_r 31,000; trypsin inhibitor, M_r 21,500; and lysozyme, M_r 14,400 (Bio-Rad Laboratories) or phosphorylase b, M_r 97,400; bovine serum albumin, M_r 66,200; ovalbumin, M_r 45,000; carbonic anhydrase, M_r 30,000; trypsin inhibitor, M_r 20,100; and α-

lactalbumin, M_r 14,400 (GE Healthcare Life Sciences). The native size of XanA isolated from each host source was estimated by gel filtration chromatography using a Protein-pak Diol(OH) 10 μm column (Waters, 0.5 or 1 min mL^{-1}, room temperature in 100 mM Tris buffer, pH 7.5, containing 300 mM NaCl), a Superose™ 6 HR 10/30 GL column (Pharmacia, 1 mL min^{-1} in 50 mM MOPS, pH 6.8, containing 0.15 M NaCl), or a Superdex 200 HR 10/30 column (Pharmacia, 0.4 mL min^{-1}, in 50 mM MOPS, pH 6.8, with 0.15 M NaCl). The calibration proteins were thyroglobulin, M_r 670,000; γ-globulin, M_r 158,000; ovalbumin, M_r 44,000; myoglobin, M_r 17,000; and vitamin B_{12}, M_r 1,350 (Bio-Rad) along with ferritin, M_r 440,000; catalase, 232,000; aldolase, M_r 158,000, and yeast alcohol dehydrogenase, M_r 150,000. A Beckman LF 3000 N-Terminal Edman sequencer (Beckman System Gold) was used in attempts to examine the *N*-terminal amino acid residues of XanA enzyme isolated from both *E. coli* and *A. nidulans*.

Analysis of Posttranslational Modifications

The XanA protein samples were tested for the presence of glycoconjugates by using the DIG Glycan Detection kit (Roche). As above, 5 μg of each protein sample was separated by 12 % SDS-PAGE, transferred to nitrocellulose, and reacted with the enzyme immunoassay reagents. In addition, XanA samples were enzymatically deglycosylated by using *N*-glycosidase F (PNGase F), an enzyme that can remove all types of *N*-linked oligosaccharides from glycoproteins (19). The enzymatic treatment was carried out with both the native and denatured XanA samples (20 μg). Denaturation was carried out in buffer containing 0.5 % SDS and 0.4 % dithiothreitol at 95 °C for 5 min (final volume, 25 μl), and then treated with 3 units of PNGase F in buffer (50 mM sodium phosphate, pH 7.5, supplemented with 1 % NP-40) at 37 °C for 2 h (final volume, 33 μl). The reactions were stopped by transferring samples onto ice, followed by 5 min at 95 °C. After digestion, samples were analyzed by SDS-PAGE and compared to protein size markers obtained from Fermentas Life Sciences.

To test for the presence and identify the types of phosphorylation in each of the XanA samples, the proteins (5 μg) were separated by 12 % SDS-PAGE and transferred to 0.45 micron nitrocellulose (Micron Separation) at 120 mA for 1 hr by using a semi-dry transfer cell (Bio-Rad). Nonspecific binding was blocked by incubating with 5 % milk protein for 1 hr before incubating with rabbit polyclonal anti-phosphoserine, rabbit polyclonal anti-phosphothreonine, or mouse monoclonal anti-phosphotyrosine antibodies (ZYMED, South San Francisco, CA) at 1 μg ml^{-1}. A horseradish peroxidase-labeled secondary antibody was then used in conjunction with an ECL Western Blotting Detection System (Amersham Biosciences, Little Chalfont Bucks, UK). The labeled immunoblot was placed against reflection autoradiography film (Kodak X-Omat XK-1) and developed 1 sec. Kaleidoscope protein size markers were obtained from Bio-Rad Laboratories.

Mass Spectrometry

Mass spectrometry analyses were performed using a Waters (Milford, MA) LCT Premier mass spectrometer coupled to a Shimadzu (Columbia, MD) LC-20AD HPLC and SIL-5000 autosampler. Samples were analyzed using electrospray ionization in positive ion mode. On-line desalting and separation from detergents was performed using a Thermo Hypersil-Keystone BetaBasic cyano column (1.0 × 10 mm) coupled to the electrospray ionization probe. Aliquots were injected onto the column using a flow rate of 0.1 mL/min of 95% solvent A (0.15% aqueous formic acid)/5% solvent B (acetonitrile). Gradient elution was performed by using the following parameters: (0-1 min: 95%A/5%B; linear gradient to 30%A/70%B at 6 min; hold at 30%A/70%B until 9 min). Electrospray spectra were processed using MassLynx software (Waters, Milford, MA), and zero-charge state mass spectra were obtained by deconvolution using the MaxEnt1 algorithm.

MALDI mass spectra were generated on a Voyager-DE STR mass spectrometer (Applied Biosystems, Foster City, CA) in positive ion linear mode using sinapinic acid as matrix. Samples were processed using strong cation exchange ZipTips (ZipTipSCX, Millipore, Billerica, MA) to remove detergent and reversed phase C18 ZipTips for desalting, following the manufacturer's recommended protocols, before spotting the MALDI target.

Enzyme Assays

Xanthine/αKG dioxygenase activity was measured at 25 °C or 30 °C (as specified in the figure legends) by using the following typical assay conditions (total volume of 1 mL): 1 mM αKG, 40 μM $Fe(NH_4)_2(SO_4)_2$, and 200 μM xanthine in 50 mM MOPS buffer, pH 7.4 or 7.0 (see figure legends). Variations of these conditions included use of alternate buffers, different pH values, and varied concentrations of substrates. The absorbance at 294 nm was monitored to determine the uric acid production (ε_{294} 12,200 M^{-1} cm^{-1}) with a correction for loss of the xanthine absorbance at this wavelength (measured ε_{294} 2,000 M^{-1} cm^{-1}) for an overall change in ε_{294} of 10,200 M^{-1} cm^{-1}. Units of activity (U) were defined as μmol min^{-1} of uric acid produced and the specific activity (U mg^{-1}) was measured as μmol min^{-1} (mg of purified XanA)$^{-1}$.

In addition to the above spectroscopic assay, xanthine/αKG dioxygenase activity was measured by two alternative methods. Oxygen consumption measurements were carried out in air-saturated MOPS medium (pH 7) at 25 °C by using a Clark-type oxygen electrode. Quantification of αKG consumed during the reaction was assessed by HPLC. Aliquots (300 μL) of the reaction mixtures were quenched by addition of 5 μL 6 M H_2SO_4, the samples were centrifuged for 5 min at 20,000 *g*, and the supernatant was chromatographed on an Aminex HPX-87H column (Bio-Rad Laboratories) in 0.013 M H_2SO_4 with detection by using a differential refractometer (Waters, Model R401). Succinate was quantified by using a succinate detection kit (Boehringer Mannheim/R-Biopharm) according to the manufacturer's instructions.

Metal Analyses

Particle induced X-ray emission (PIXE) experiments were carried out in a tandem Pelletron accelerator, using a 3 MeV proton beam of 1 mm diameter at the sample surface. The XanA enzyme was dialyzed in 50 mM NH_4HCO_3, dried on a 3.5 μm Mylar membrane, and the X-ray emission was detected in two solid-state detectors: a Si-pin Amptek (180 eV-resolution operated under helium stream) and for heavier elements a LE Ge detector with a 38 μm Al foil absorber (20,21). Spectra were collected for 5 min, using at least in two sites within each sample. Sulfur was taken as an internal standard, taking into account that the enzyme subunit contains 7 S atoms per polypeptide chain, including 2 cysteine and 5 methionine residues. An alternative approach to measure the iron concentration utilized the $KMnO_4$ oxidation, ascorbate reduction, and ferrozine chelation protocol of Beinert (22).

Sources and Synthesis of Chemical Analogues of αKG and Xanthine

αKG, α-ketoadipate, α-ketobutyric acid, pyruvate, phenylpyruvate, 4-hydroxyphenylpyruvate, purine, 6-methylpurine, 2-hydroxypurine, 2-hydroxy-6-methylpurine, hypoxanthine, xanthine, 1-methylxanthine, 3-methylxanthine, 7-methylxanthine, 9-methylxanthine, allopurinol, and allantoin were from Sigma-Aldrich. *N*-oxalylglycine (NOG) was a gift from Dr. Nicolai Burzlaff.

8-Hydroxypurine and 6,8-dihydroxypurine (6,8-DHP) were prepared from the commercially available (Sigma Aldrich) 4,5-diaminopyrimidine and 4,5-diamino-6-hydroxypyrimidine, respectively, following a modified method described previously (23). 2,8-Dihydroxypurine (2,8-DHP) was prepared following a published method (24).

8-^{2}H-Xanthine Preparation

8-^{2}H-xanthine was prepared by incubating a 1 % (w/v) xanthine solution in ^2H_2O (99.9 %, Sigma & Aldrich), with 0.3 M NaO^2H (> 99 % ^{2}H, Sigma-Aldrich) in a serum vial sealed with a butyl rubber stopper for 20 h in a 100 °C oven. The proton-deuterium exchange was monitored by using NMR spectroscopy to integrate the resonance at 6.9 ppm due to the proton on C-8. The final solution was diluted and neutralized to pH 7.0. The 8-^{2}H-xanthine precipitated from the solution and was dried under vacuum for at least 3 h. Yields were approximately 90 %. The purity of 8-^{2}H-xanthine was monitored by electrospray ionization mass spectrometry, and the conversion was shown to be 98.4 % as a molar ratio.

^2H_2O Solvent Isotope Effect

In 1 mL 50 mM MOPS, p^{2}H 8.0 (p^{2}H values were determined by adding 0.4 to the pH 7.6 electrode reading), 0.51 μg of purified XanA was assayed in 40 μM $Fe(NH_4)_2(SO_4)_2$, 1 mM αKG and 0-200 μM xanthine. All buffers were prepared in ^2H_2O. These data were compared to assays carried out in the same conditions at pH 7.6. Of note, the *E. coli*-derived enzyme exhibits optimal activity over a range from pH 7.0 to 8.0.

Fluorescence Spectroscopic Analysis of XanA

Fluorescence measurements were made on an ISS PC1 spectrofluorimeter (Champaign, IL, U.S.A.). The temperature of the cells was maintained at 30 °C. Fluorescence measurements were carried out at an excitation wavelength of 280 nm (0.5 nm band-width) with emission monitored from 300 to 400 nm (2 nm bandwidth).

Structural Modeling

A homology model of XanA was generated on the basis of the structure of the related enzyme TauD (PDB code 1OTJ, chain A, and PDB code 1OS7, chain A) (25). XanA is 18 % identical to TauD over 280 residues, and has three significant additional regions of 15, 22, and 18 amino acids. Multiple templates for the XanA structure were obtained with PSI-BLAST (26,27) starting both from the amino acid sequence of XanA and from that of several closely related proteins for which no structure has yet been reported, and with 3D-Jury (28) using the Bioinfo Meta Server (http://bioinfo.pl/Meta). Additional suboptimal alignments for each template were generated using probA (29) to produce a large pool of possible models. A structural model was constructed from each alignment, with side chains reconstructed using the MMTSB Tool Set (30,31), and the best model from the entire set of models was selected according to combined energy scores from DFIRE (32), MMGB/SA (33), and RAPDF (34), using a correlation-based approach (35) in combination with clustering. The αKG and iron were placed into the active site according to the TauD structure.

RESULTS

Purification of XanA from the Bacterial Host

XanA produced in *E. coli* XL1Blue (pxan-His_6) was purified to homogeneity from cell extracts (Figure 1 and Figure S1, Supporting Material) by Ni-NTA chromatography. Inclusion of 15 % glycerol in the chromatography buffers, which were maintained on ice, helped to minimize protein precipitation during purification. About 5 % of the soluble activity was located in the flow-though fractions, perhaps indicating that some XanA interacts tightly with other proteins that fail to bind the resin. As measured by the standard assay protocol, the Ni-NTA column fractions containing purified XanA accounted for 33 % of the activity that had been observed in cell extracts. When this pool was treated with 1 mM EDTA at 4 °C for 5 h and then concentrated to 5-12 mg mL^{-1}, the activity increased such that 60 % of the activity of cell extracts was recovered and yielded a final specific activity for the purified enzyme of 70-80 U

(mg protein)$^{-1}$ at 25 °C which corresponds to a k_{cat} of 49-56 s^{-1} (assuming M_r = 42 kDa per subunit). The enzyme recovered from the Ni-NTA column contained 0.26 to 0.5 moles of Fe per mole of subunit according to the colorimetric assay, while that incubated with EDTA lacked detectable Fe, and a sample incubated with exogenous Fe^{II} and then chromatographed on a Sephadex G-25 gel filtration column contained 1.3 moles of Fe per mole of subunit. Concentrated XanA derived from *E. coli* was stable for at least one month at 4 °C when stored in 100 mM Tris buffer, pH 8.0, containing 300 mM NaCl, 250 mM imidazole, 1 mM EDTA and 15 % glycerol, or at least two months if frozen at -80 °C. Additionally, the enzyme was stable for one month at 4 °C when stored in 100 mM Tris buffer, pH 7, containing 300 mM NaCl, 250 mM imidazole, 15 % glycerol, and 5 μM Fe^{II}.

Purification of XanA from the Fungal Host

In a similar manner, His_6-tagged XanA was purified to homogeneity (Figure 1) from extracts derived of the *A. nidulans* mycelia by using immobilized metal ion affinity chromatography. To stabilize the enzyme and the activity, 5 μM Fe^{II} was added to the purified enzyme pool. The specific activity of the isolated protein was measured as 22-40 U (mg protein)$^{-1}$ at 30 °C equivalent to a k_{cat} of 15.4-30 s^{-1} (again assuming M_r = 42 kDa per subunit). Metal analyses by PIXE (Figure S2, Supporting Information) indicated 1.13 ± 0.2 moles of Fe per mole of enzyme subunit, with trace levels of Ni and Zn that are likely to derive from the Ni-NTA column and from contamination, respectively. Concentrated XanA derived from *A. nidulans* was stable for at least 5 months at 4 °C when stored in 100 mM Tris buffer, pH 7, containing 300 mM NaCl, 250 mM imidazole, 15 % glycerol, and 5 μM Fe^{II}.

Differential Protein Properties of XanA Purified from the Two Host Cells

The SDS-PAGE results described above highlight a key difference between the XanA proteins isolated from the two sources; i.e., the apparent M_r of the *E. coli*-derived protein is larger than that of the protein derived from the fungus (Figure 1). This finding led us to investigate other properties of the two proteins. Efforts to obtain *N*-terminal sequences were unsuccessful, consistent with the amino termini of both proteins being blocked. Gel filtration chromatography provided an estimated M_r of 39-42 kDa for the native enzyme isolated from the bacterial host (consistent with a monomeric structure); however, similar analysis of the protein from the fungal host showed that it was oligomeric, with an approximate M_r of 500 kDa that was consistent with about twelve subunits per native molecule (Figure S3, Supporting Information). The observed differences in the samples hinted at the possibility of unique posttranslational modifications in the proteins produced in the bacterial and eukaryotic hosts.

XanA samples derived from the two sources were each tested for the presence of bound carbohydrate. The protein purified from *A. nidulans*, but not that isolated from *E. coli*, was shown to be glycosylated (Figure 2). It is noteworthy that removal of glycosyl residues from the fungus-derived protein resulted in a significantly lower apparent molecular mass than that of the enzyme isolated from *E. coli*, suggesting a truncation occurs in the fungal host (see below). Specifically, treatment of the native XanA enzyme from *A. nidulans* with the *N*-glycosylase PNGase F led to a shift in the denaturing gel electrophoretic mobility (Figure 2) from a form with apparent M_r of more than 40 kDa to one with apparent M_r near 33 kDa, indicating removal of *N*-glycosylation. The PNGase F-treated protein was still detected by the glycoconjugate immunoassay. These results are consistent with the presence of *O*-glycosylation in the protein, as well as the *N*-glycosylation that is removed by PNGase F. As a control, the native and denatured XanA prepared from *E. coli* was subjected to PNGase F treatment and no shift in mobility was detected in either sample.

In addition, the samples were tested for phosphorylation. Figure S4 (Supporting Information) illustrates the reactions of both proteins with antibodies that recognize specific types of

phosphorylated amino acids. The enzyme purified from *E. coli* reacted strongly with both anti-phosphoserine and anti-phosphothreonine antibodies, while the enzyme purified from *A. nidulans* reacted strongly with the anti-phosphothreonine antibodies and only weakly with the anti-phosphoserine antibodies. Neither protein sample reacted with anti-phosphotyrosine antibodies.

Mass spectrometric methods were used to further characterize the two enzyme forms. Electrospray ionization mass spectrometry of bacteria-derived XanA indicated a single species with a molecular mass of 41,992 Da (data not shown), which matches very well to the theoretical mass (41,996.50 Da; using the ExPASY Compute pI/Mw tool at ca.expasy.org) for the His_6-tagged protein missing its amino-terminal Met residue. This sample provided no evidence of phosphorylation, perhaps arising from subtle differences in bacterial culture conditions in our two different laboratories. In contrast to this single species, the fungus-derived protein sample exhibited a complex electrospray ionization mass spectrum centered near 36,000 Da (Figure 3) in agreement with the results from matrix-assisted laser desorption-ionization mass spectrometry (data not shown). The spectrum of Figure 3 includes features separated by 162 mass units, consistent with glycosylation involving hexose sugars, as well as features separated by 80 mass units, indicating phosphorylation. The smallest component of the spectrum exhibits a mass of 35,171 Da, indicating that the non-glycosylated and non-phosphorylated fungal protein is severely truncated compared to the theoretical mass of full-length protein of 42,127.69. This truncation, consisting of approximately 60 residues, must occur at the N-terminus, since the C-terminal His_6-tag was used for enzyme purification.

Effects of pH on Stability and Activity of Xanthine/αKG Dioxygenase

The effect of pH on the stability of XanA was examined for the enzyme isolated from each source. After incubating the XanA samples in various pH buffers at 4 °C for 3 h, the activity remaining was examined by using the standard assay procedure. The results (data not shown) indicate that each purified enzyme is stable over a wide pH range (7.0-11.0).

Two methods were used to examine the effects of pH on the activity of the two forms of enzyme. XanA isolated from *E. coli* was assayed by using a series of different buffers and shown to exhibit a narrow pH optimum of 7.0-8.0 with pH 7.4 yielding optimal activity for Tris, MOPS, MES, imidazole, and HEPES buffers (Figure S5, upper panel, Supporting Information). For the XanA isolated from *A. nidulans*, a constant ionic strength, three-buffer system containing 0.1 M MOPS, 0.52 M Tris, and 0.052 M ethanolamine (36) provided a sharp maximal activity at pH 7.0 (Figure S5, lower panel).

Kinetic Analyses and Stoichiometry of XanA

The kinetic parameters were very similar for XanA isolated from the two sources. For the *E. coli*-derived enzyme, the results of studies using varied αKG concentrations provided a K_m of 31.1 ± 1.6 μM and k_{cat} of 66.5 s^{-1} at 25 °C (Figure 4A), while those for varied xanthine concentrations provided a K_m of 45.2 ± 3.6 μM and k_{cat} of 71.4 s^{-1} (Figure 4B). Similarly, when the protein isolated from *A. nidulans* enzyme was assayed at 30 °C with varied αKG or xanthine concentrations the measured K_m values were 50 μM ± 6 and 46 ± 4 μM, respectively, but with a smaller k_{cat} that ranged from 15 s^{-1} to 30 s^{-1} depending on the preparation.

The stoichiometry of the enzymatic reaction was examined for XanA from each source. Using the fungus-derived protein, the degradation of 120 μM xanthine was accompanied by the production of 110 μM uric acid, and this coincided with the consumption of 130 μM oxygen and the production of 185 μM succinate. The larger changes in the amount of oxygen and succinate compared to those of xanthine and uric acid are consistent with a well-known phenomena reported for this class of enzymes in which substrate hydroxylation can be partially

uncoupled from oxidative decarboxylation (37-40). An analogous near coincidence between xanthine consumption, uric acid production, and oxygen consumption was observed for the bacteria-derived sample (results not shown).

Isotope Effects

To test for substrate or solvent isotope effects on the overall reaction rate, activity assays were carried out by using 8-^{2}H-xanthine or in $^{2}H_2O$ and compared to control studies with unlabeled xanthine in H_2O. No significant isotope effect was observed when the reaction was carried out with 8-^{2}H-xanthine (98.4 % enriched with ^{2}H) and compared to non-labeled substrate (data not shown). In contrast, a significant solvent deuterium isotope effect was observed (Figure 5), with V_{max} reduced by 50 % (72.1 U mg^{-1} dropping to 34.0 U mg^{-1}) while K_m was nearly unaffected (45.2 and 48.9 mM, respectively).

Metal Ion Dependence of XanA

The metal dependence of the reaction was examined with enzyme samples derived from the two sources. Fe^{II} is required for xanthine/αKG dioxygenase activity, with half-maximal activity at ~7 μM when using the apoprotein isolated from the bacterium (Figure 6). Depending on the experimental conditions, Fe^{II} concentrations greater than 25 μM can lead to enzyme inhibition of XanA isolated from *E. coli*, whereas the enzyme from *A. nidulans* was not inhibited at Fe^{II} concentrations up to 80 μM.

Metal ions other than Fe^{II} were tested and found to be unable to stimulate activity when added to the apoprotein (data not shown). When various metal ions were added to the assay buffer in concentrations equivalent to that of Fe^{II}, both Cu^{II} and Zn^{II} completely inhibited the xanthine/αKG dioxygenase activity, with partial inhibition observed with Co^{II}, Mn^{II}, and (much less pronounced) Ni^{II} (Figure 7). The inactive metal ions are presumed to compete for the Fe^{II}-binding site.

Effect of Salt on XanA Activity

The activity of XanA isolated from the bacterial source was shown to decrease in buffers containing NaCl (Figure S6, Supporting Material). Kinetic analyses revealed that 0.5 M NaCl salt increased the K_m of αKG to 0.74 ± 0.08 mM, increased the K_m of xanthine to 105 ± 5.8 μM, and decreased the k_{cat} to 35.4 s^{-1} and 43.2 s^{-1}, respectively in the two studies. These findings indicate that the K_m of αKG is significantly affected by ionic strength, while the K_m of xanthine and k_{cat} are less affected, and demonstrate that the salt content of fractions recovered during protein isolation must be considered when assaying the enzyme.

αKG Analogues

In addition to αKG, α-ketoadipic acid is a cosubstrate of XanA and results in an activity of 9.2 U (mg protein)$^{-1}$ or about 1/10 of that observed with αKG, when examined using the *E. coli*-derived protein. Kinetic analyses revealed a k_{cat} of 7.6 s^{-1} and a K_m of 0.16 mM for this alternative cosubstrate compared to a k_{cat} of 61 s^{-1} and K_m of 31 μM for αKG. In contrast, pyruvate, α-ketobutyric acid, phenylpyruvate, and 4-hydroxyphenylpyruvate were not used as cosubstrates. NOG, a known inhibitor of several Fe^{II}/αKG-dependent dioxygenase family members (41-45), was shown to compete with αKG and provided a K_i of 0.12 μM for inhibition when tested with the bacteria-derived enzyme (Figure 8).

Xanthine Analogues

XanA was shown to be highly specific for xanthine. On the basis of the spectroscopic assay using standard conditions with 12 nM enzyme, no activity was detected when the enzyme was assayed with 80, 100, or 200 μM hypoxanthine, 1-methylxanthine, 3-methylxanthine, 7-

methylxanthine, 9-methylxanthine, purine, 6-methylpurine, 2-hydroxypurine, 8-hydroxypurine, 2,8-dihydroxypurine, 2-hydroxy-6-methylpurine, allopurinol, allantoin, or adenosine diphosphate. Similarly, significant inhibitory effects were not observed with 100 or 200 μM of any of these compounds (although very modest inhibition was noted with 2,8-DHP). The one xanthine-like compound that does significantly inhibit the enzyme, but does not serve as a substrate, is 6,8-DHP. When bacteria-derived XanA was assayed by using standard conditions supplemented with 80 μM 6,8-DHP, the activity decreased by 24 % when the reaction was initiated by enzyme addition, or by 60%, if the reaction was initiated by adding xanthine. Fungus-derived XanA appeared to be even more sensitive to the presence of this inhibitor (data not shown). Although the kinetic mechanism of inhibition by this compound currently is unclear, the affinity of the enzyme samples for this compound was further examined by fluorescence measurements.

Fluorescence Spectroscopic Analysis of XanA

The binding of αKG, xanthine, and 6,8-DHP to both the bacterial- and fungal-derived proteins was examined by monitoring changes in the endogenous fluorescence of the proteins (Figure S7, Supporting Data). Fitting of the plots of change in fluorescence intensity versus ligand concentration revealed that the two proteins exhibited very similar K_d values for xanthine (110 ± 19 μM and 220 ± 19 μM for the bacterial- and fungal-derived samples), αKG (29 ± 4 μM and 17 ± 4 μM, respectively), and 6,8-DHP (60.5 ± 9 μM and 156 ± 16 μM). Of interest, the αKG K_d happens to be very similar to the K_m of this compound measured during catalysis. The measured K_d of 6,8-DHP confirms that this compound binds to the protein even in the absence of Fe^{II} and αKG.

Homology Model of XanA

XanA was aligned with TauD and the structure of that protein (25,46) was used as the template to create a homology model. The overall sequence identity is 18%, however the sequence identity of the most relevant structural regions near the active site is 33%. Moreover, given recent advances in structure prediction, sequence identities as low as 18% identity are commonly sufficient to support comparative modeling with a good match of predicted secondary structure elements (47,48) as in the case of XanA. Consequently, it is reasonable to assume that our model of the XanA structure captures the overall features correctly, while structural details near the active site are likely represented more accurately. Nevertheless, we acknowledge that any predicted model without further experimental validation remains speculative and is subject to some level of uncertainty.

As illustrated in Figure 9, the XanA protein is predicted to contain the double-stranded β-helix fold comprised of eight β-strands with connecting loops, as is typical of this enzyme family (6,49). Three loops in the sequence, comprising residues 72-88, 173-190, and 219-231, had no counterparts in TauD and were not modeled (indicated by boxes at the appropriate positions in the figure), but these are all distant from the putative active site region. The homology model contains the Fe^{II}-binding site (His149, Asp151, and His340) expected from prior sequence alignments (2). The cosubstrate (shown in yellow) was positioned into the model so as to chelate Fe^{II} in a similar fashion as αKG occurs in TauD. The KG C-5 carboxylate is predicted to form a salt bridge with Arg352 (depicted in red), while Lys122 (in green) is well positioned to stabilize the C-1 carboxylate of the cosubstrate.

DISCUSSION

In this study we describe the isolation and general characterization of xanthine/αKG dioxygenase, a novel enzyme found exclusively in the fungal kingdom (2). Immobilized metal ion chromatography proved to be very effective for purifying recombinant XanA from either

the bacterial or fungal host cells. As described below, the two forms of the protein differed markedly in their properties, but were very similar in their enzymatic properties.

Posttranslational Modifications

Our comparison of recombinant XanA purified from *E. coli* and *A. nidulans* reveals very different quaternary structures and posttranslational modifications. Whereas the protein derived from the bacterial source is a monomer, that isolated from the fungus is much larger, with apparent M_r of 500 kDa. Both protein samples are at least partially phosphorylated, but the sample from the fungus is also glycosylated. Treatment of the latter protein with PNGase F results in a dramatic shift in electrophoretic mobility, but not all glycosylation is removed by this process indicating the presence of both *N*- and *O*-glycoconjugates. The smaller electrophoretic species is consistent with the size of the protein determined by mass spectrometric methods. These results suggest an extensive truncation takes place at the N-terminus of the fungus-derived enzyme. Analogous biochemical comparisons between the enzyme form isolated from its native eukaryotic host and the form isolated from a heterologous host, such as the *E. coli* used here, have not been reported for other Fe^{II}/αKG dioxygenase family members.

An extant question is the role of the extensive N-terminal processing of enzyme isolated from its natural fungal host. We speculate that this feature may relate to cellular targeting of the XanA enzyme. It is not unreasonable to propose that an oxidoreductase such as XanA could be peroxisomal. In fact, the immediate downstream enzyme, urate oxidase, has been shown to be peroxisomal in every organism where its localization has been investigated, including amoebas, mammals and plants (50-53). A urate oxidase-green fluorescent protein fusion shows a particulate intracellular distribution in *Aspergillus nidulans*, fully consistent with a peroxisomal localization (G. Langousis and G. Diallinas, unpublished data). XanA does not possess a C-terminal peroxisomal targeting signal (variations of an SKL tripeptide, denoted PTS1); however, it contains a RSALYTHL sequence (residues 40-47) that resembles the PTS2 N-terminal import sequence (variations of RLX_5HL) found in a minority of peroxisomal proteins throughout the eukaryotes (54-56). In some instances, including mammalian (57), yeast (58), and plant (59) peroxisomal proteins, it has been shown that the PST2 is contained in a pre-sequence that is cleaved upon peroxisomal entry. The function of XanA glycosylation could be understood in this context as a mechanism to protect the protein from further proteolysis.

Insights into the Post-Translational Modifications from the XanA Homology Model

The XanA homology model (Figure 9) provides useful insights into the likely sites of posttranslational modification (Figure S8, Supporting Information). The model is based on the full-length sequence, but we assume the overall fold is maintained even in the truncated version derived from the fungal host because this extension is external to the double-stranded β-helix core. Consistent with our PNGase F results that demonstrate the presence of *N*-glycosylation sites in the fungus-derived protein, the NetNGlyc 1.0 server (R. Gupta, E. Jung, and S. Brunak, unpublished) predicts glycosylation of Asn118, and the model places this residue on the protein surface. The PNGase F-treated fungal-derived protein still stains as a glycoprotein, consistent with *O*-linked glycoconjugates in the protein. Thr5 and Thr10 are predicted to be glycosylated by the NetOGlyc 3.1 server (60) while the YingOYang 1.2 server (R. Gupta, J. Hansen, and S. Brunak, unpublished) predicts Thr5, Ser37, Thr195, Ser231, and Ser316 as possible sites of glycosylation. The XanA homology model has these positions surface exposed except for Thr195. On the basis of our mass spectrometry results showing truncation of approximately 60 residues from the N-terminus, we suggest Ser231 or Ser316 as the most likely sites of O-glycosylation.

A wide range of potential Ser, Thr, or Tyr phosphorylation sites are identified in XanA by the NetPhos 2.0 server (61) and by Prosite (www.expasy.org). Phosphoproteins are common in eukaryotes and are well known in *E. coli* (62). Thr phosphorylation sites are predicted by at least one program to include Thr5, Thr38, Thr58, Thr66, Thr120, Thr177, and Thr274. The first three residues are missing in the fungus-derived protein based on the mass spectrometry results. The homology model predicts that Thr66 and Thr120 are buried, whereas the other residues are exposed to the surface. The bacteria-derived protein also reacts with antibodies directed against phosphoserine, whereas XanA derived from the fungus reacted only weakly with these antibodies. We attribute this difference in reactivity between the two proteins to the phosphorylation site being inaccessible in the fungal-derived sample, due to nearby glycosylation or to being located at a subunit interface in the multimeric protein. Predicted sites of Ser phosphorylation include Ser15, Ser37, Ser142, Ser184, Ser199, Ser208, Ser217, Ser218, and Ser341. The first two residues are absent in the fungus-derived protein. Residues Ser199 and Ser341 are predicted to be somewhat buried in the model, Ser184 occurs on a loop that could not be modeled, and the other residues are predicted to be surface exposed. Of note, Ser341 would be made more inaccessible by glycosylation of Thr195; thus, potentially explaining the source specificity behavior for Ser phosphorylation.

General Aspects of XanA Activity

Purified XanA is unstable at room temperature (denaturing within an hour even in buffers containing 15 % glycerol), when agitated (e.g., during stirring in an Amicon concentrator), or when incubated at pH values below 6.5 (the pI estimated for XanA is 5.82 according to the ExPASy ProtParam tool at ca.expasy.org). EDTA treatment enhances the activity of the highly concentrated bacteria-derived enzyme and this compound is maintained in the storage buffer to ensure maximal lifetime of the activity. We attribute the enhancement effect of EDTA to its ability to remove inhibitory Ni^{II} (co-eluted with the enzyme from the NTA resin) and Fe^{III} (the oxidized, inactive state of the metal) from the enzyme so that the apoprotein can bind Fe^{II} in the assay buffer. Several other Fe^{II}/αKG dioxygenases are purified as their apoprotein forms by inclusion of chelators (63,64). In contrast, some representatives of these enzymes have been purified anaerobically to assure that the metal remains in its reduced form (65,66).

The kinetic properties of XanA as purified from *E. coli* (~70 U mg^{-1}, K_m of 31 μM for αKG, and K_m of 45 μM for xanthine at pH 7.4) compare well with those of XanA isolated from *A. nidulans* (30 U mg^{-1}, and K_m values of 50 μM and 46 μM at pH 7.0), and these results are compatible with those reported earlier for enriched sample from the fungus (40 U mg^{-1}, 50 μM, and 23 μM) (2). Although the xanthine C-H bond is broken at C-8 during turnover, substitution of the proton at this position by ^2H did not lead to a substrate isotope effect. This result demonstrates that C-H cleavage is not the rate-determining step in the reaction. The deuterated substrate might be useful in future experiments to examine individual steps in the reaction by using transient kinetic approaches, as was elegantly demonstrated with deuterated substrate and stopped-flow techniques for TauD (67) and, more recently, prolyl 4-hydroxylase (68). In contrast to the situation with labeled xanthine, a solvent isotope effect was observed upon substituting H_2O with D_2O (Figure 5). This substitution had little effect on the K_m of xanthine while decreasing V_{max} by 40 % compared to the assay in H_2O. This result suggests that a chemical group possessing an exchangeable proton is important in the rate-determining step of the overall reaction. Options for the protonatable group include a general base or general acid protein side chain or a metallocenter species such as Fe^{III}-OOH or Fe^{III}-OH. The finding of a solvent deuterium isotope effect contrasts with the case of TauD, where product release is the slow step in catalysis and no solvent isotope effect is observed (12,63).

The reaction requires Fe^{II} (half-maximal activity at 7 μM for standard conditions), consistent with the results of related family members. Zn^{II} and Cu^{II} are potent inhibitors of XanA, and

several other metals also inhibit the enzyme (Figure 7). This situation resembles that known for related enzymes such as TauD where Co^{II} and Ni^{II} inhibition has been studied (41), clavaminate synthase where Co^{II} inhibition was characterized (69), or TfdA where the Cu^{II}-inhibited enzyme was analyzed (70). The inhibitory metal ions are likely to substitute for Fe^{II} and presumably utilize the same set of amino acid side chain ligands.

The inhibitory effects of NaCl on XanA observed here represent, to our knowledge, the only systematic characterization of any salt effect on an Fe^{II}/αKG dioxygenase. The presence of salt leads to a large increase in K_m of αKG, a small increase in K_m of xanthine, and a reduction in k_{cat}. We attribute the K_m effect to the ability of salt to interfere with salt bridge formation and other stabilizing interactions between αKG or xanthine and the protein. Similar salt effects are likely to apply to a wide range of other family members; thus, one must exercise caution in the choice of ionic strength when doing enzyme assays.

Co-Substrate and Substrate Specificity

The cosubstrate specificity of XanA is somewhat more relaxed than that for the primary substrate, with α-ketoadipic acid (with one extra carbon compared to αKG) also yielding activity. The increase in K_m and decrease in k_{cat} for the incorrectly-sized analogue is easily rationalized in terms of the XanA homology model where both the C-1 and C-5 carboxylates of αKG are predicted to interact with the protein (with Lys122 and Arg352, respectively) while also chelating the active site metal ion. Alternative α-ketoacids are known to support αKG-dependent activities of several other enzyme family members including TauD, TfdA, RdpA, SdpA, and an alkyl sulfatase (11,64,71,72). The αKG homologue NOG is a competitive inhibitor of XanA (Figure 8), consistent with its known inhibition of several other representatives of the Fe^{II}/αKG-dependent hydroxylases. Of interest, the measured K_i of NOG for XanA (0.12 μM) is well below the K_m of αKG in this enzyme and much below the reported 290 μM K_i for inhibition of TauD (41). More generally, the K_i of NOG can vary widely among family members (e.g., it is reported to be 1.9-7.0 μM for collagen prolyl 4-hydroxylase (42) and 1.2 mM for an oxygen-sensing asparaginyl hydroxylase (45)), presumably due to distinct interactions with the active site protein side chains in the target enzymes.

XanA proved to be exquisitely specific to its primary substrate. For example, allopurinol (a known substrate and inhibitor of xanthine oxidase (73)), 1-methylxanthine and 2-hydroxy-6-methylpurine (alternative substrates of the Moco-containing enzyme (74,75)), and several other purine-type compounds were neither substrates nor inhibitors of XanA. Of the compounds tested, only 6,8-DHP bound tightly to the enzyme. For comparison, other members of the Fe^{II}/αKG-dependent dioxygenases range widely in their substrate specificities. The prolyl hydroxylases involved in the hypoxic response appear to be highly specific for recognizing a single prolyl residue in the HIF1 α protein (76,77). By contrast, TfdA utilizes a wide range of phenoxyacetic acids (64) and a yeast αKG/sulfonate dioxygenase metabolizes a diverse array of sulfonates (78).

Insights into Substrate Binding from the XanA Homology Model

Additional structural or mutagenesis studies are required to characterize the mode of substrate binding to XanA; however, our homology model (Figure 9) allows us to identify potential key active site residues (Figure S9, Supporting Information). The model depicts a pocket adjacent to the metallocenter and lined by a series of putative active site residues (Gln99, Pro100, Gln101, Ile110, Thr120, Lys122, Glu137, Ala152, Leu154, Gln356, and Asn358) that are generally well conserved in sequences of XanA orthologues (Figure S10, Supporting Information). Pro100, Gln101, Gln356, and Asn358 are universally conserved in XanA sequences. Gln99 counterparts are often present, but Val occupies this position in some representatives. Lys122, which could stabilize the αKG C-1 carboxylate as well as bind

substrate, either is retained or conservatively replaced by Arg or Thr. In some fungi, various residues (Lys, Gln, Arg, Asn, and Glu) replace Thr120, but all of these are able to function in hydrogen bonding. Similarly, Asp, Gln, or Ser, all capable of similar hydrogen bond interactions, replace Glu137 in other XanA homologues. Among the hydrophobic residues predicted to surround the active site, Ile110 is replaced by Val or Phe, Ala152 is replaced by Ser in one case, Leu154 is strictly conserved, and Leu251 (for clarity, this is not shown in Figure S9 because it lies on top of Pro100) is retained or replaced by other large side chains in other orthologues. Aromatic groups, often involved in π-π stacking interactions with nucleic acids and known to occur in xanthine hydroxylase (8,79) and uric acid oxidase (80), do not appear to be important for binding xanthine in xanthine/αKG dioxygenase on the basis of this model. These predictions set the stage for future chemical modification, mutagenesis, and structural efforts to examine the substrate binding interactions.

Supplementary Material

Refer to Web version on PubMed Central for supplementary material.

ACKNOWLEDGMENT

We thank Mario Calcagno for providing laboratory facilities to GMMM, Antonietta Cultrone for generous help at the outset of this work, Christine Drevet for the alignment of XanA with putative orthologous sequences from several fungi, and Nicolai Burzlaff for providing NOG. We also thank the generous help of José L. Ruvalcaba-Sil for the PIXE analyses, Laura Palomares for the glycosylation analyses, Guillermo Mendoza-Hernandez for the N-terminal Edman degradation analyses, Dan Jones for mass spectrometry assistance, and George Diallinas for allowing us to quote unpublished data from his laboratory.

REFERENCES

1. Hille R. Molybdenum-containing hydroxylases. Arch. Biochem. Biophys 2005;433:107–116. [PubMed: 15581570]
2. Cultrone A, Scazzocchio C, Rochet M, Montero-Moràn G, Drevet C, Fernàndez-Martìn R. Convergent evolution of hydroxylation mechanisms in the fungal kingdoms: molybdenum cofactor-independent hydroxylation of xanthine via a-ketoglutarate dependent dioxygenase. Molec. Microbiol 2005;57:276–290. [PubMed: 15948966]
3. Darlington AJ, Scazzocchio C. Evidence for an alternative pathway of xanthine oxidation in *Aspergillus nidulans*. Biochim. Biophys. Acta 1968;166:557–568. [PubMed: 5680610]
4. Sealy-Lewis HM, Scazzocchio C, Lee S. A mutation defective in xanthine alternative pathway of *Aspergillus nidulans*: its use to investigate the specificity of *uaY* mediated induction. Molec. Gen. Genet 1978;164:303–308. [PubMed: 362158]
5. Cultrone A, Reyes-Dominguez Y, Drevet C, Scazzocchio C, Fernàndez-Martìn R. The tightly regulated promoter of the *xanA* gene of *Aspergillus nidulans* is included in a helitron. Molec. Microbiol. 2007in press
6. Hausinger RP. Fe(II)/a-ketoglutarate-dependent hydroxylases and related enzymes. Crit. Rev. Biochem. Mol. Biol 2004;39:21–68. [PubMed: 15121720]
7. Glatigny A, Hof P, Romao MJ, Huber R, Scazzocchio C. Altered specificity mutations define residues essential for substrate positioning in xanthine dehydrogenase. J. Mol. Biol 1998;278:431–438. [PubMed: 9571062]
8. Truglio JJ, Theis K, Leimkühler S, Rappa R, Rajagopalan KV, Kisker C. Crystal structure of the active and alloxanthine-inhibited forms of xanthine dehydrogenase from *Rhodobacter capsulatus*. Structure 2002;10:115–125. [PubMed: 11796116]
9. Goudela S, Karatza P, Koukaki M, Frilingos S, Diallinas G. Comparative substrate recognition by bacterial and fungal purine transporters of the NAT/NCS2 family. Molec. Membrane Biol 2005;22:263–275.

10. Koukaki M, Vlanti A, Goudela S, Pantazopoulou A, Gioule H, Tournaviti S, Diallinas G. The nucleobase-ascorbate transporter (NAT) signature motif in UapA defines the function of the purine translocation pathway. J. Mol. Biol 2005;350:499–513. [PubMed: 15953615]
11. Eichhorn E, van der Ploeg JR, Kertesz MA, Leisinger T. Characterization of a-ketoglutarate-dependent taurine dioxygenase from *Escherichia coli*. J. Biol. Chem 1997;272:23031–23036. [PubMed: 9287300]
12. Grzyska PK, Ryle MJ, Monterosso GR, Liu J, Ballou DP, Hausinger RP. Steady-state and transient kinetic analyses of taurine/a-ketoglutarate dioxygenase: effects of oxygen concentration, alternative sulfonates, and active site variants on the Fe(IV) intermediate. Biochemistry 2005;44:3845–3855. [PubMed: 15751960]
13. Saari RE, Hausinger RP. Ascorbic acid-dependent turnover and reactivation of 2,4-dichlorophenoxyacetic acid/a-ketoglutarate dioxygenase using thiophenoxyacetic acid. Biochemistry 1998;37:3035–3042. [PubMed: 9485456]
14. Liu A, Ho RYN, Que L Jr. Ryle MJ, Phinney BS, Hausinger RP. Alternative reactivity of an a-ketoglutarate-dependent iron(II) oxygenase: enzyme self-hydroxylation. J. Am. Chem. Soc 2001;123:5126–5127. [PubMed: 11457355]
15. Ryle MJ, Liu A, Muthukumaran RB, Ho RYN, Koehntop KD, McCracken J, Que L Jr. Hausinger RP. O_2- and a-ketoglutarate-dependent tyrosyl radical formation in TauD, an a-keto acid-dependent non-heme iron dioxygenase. Biochemistry 2003;42:1854–1862. [PubMed: 12590572]
16. Henshaw TF, Feig M, Hausinger RP. Aberrant activity of the DNA repair enzyme AlkB. J. Inorg. Biochem 2004;98:856–861. [PubMed: 15134932]
17. Bradford MM. A rapid and sensitive method for the quantitation of microgram quantities of protein utilizing the principle of protein-dye binding. Anal. Biochem 1976;72:248–254. [PubMed: 942051]
18. Laemmli UK. Cleavage of structural proteins during the assembly of the head of bacteriophage T4. Nature (London) 1970;227:680–685. [PubMed: 5432063]
19. Maley F, Trimble RB, Tarentino AL, Plummer TH Jr. Characterization of glycoproteins and their associated oligosaccharides through the use of endoglycosidases. Anal. Biochem 1989;180:195–204. [PubMed: 2510544]
20. Garman E. Leaving no element of doubt: analysis of proteins using microPIXE. Structure 1999;7:R291–R299. [PubMed: 10647175]
21. Garman EF, Grime GW. Elemental analysis of proteins by microPIXE. Prog. Biophys. Molec. Biol 2005;89:173–205. [PubMed: 15910917]
22. Beinert H. Micro methods for the quantitative determination of iron and copper in biological material. Meth. Enzymol 1978;54:435–445. [PubMed: 732579]
23. Albert A, Brown DJ. Pruine studies. Part I. Stability to acid and alkali. Solubility. Ionization. Comparison with pteridines. J. Chem. Soc 1954:2060–2071.
24. Dornow, a.; Hinz, E. Syntheses of nitrogen-containing heterocycles. XVIII. ortho-condensations of heterocyclic *o*-aminocarboxylic acid derivatives. Chem. Ber 1958;91:1834–1840.
25. O'Brien JR, Schuller DJ, Yang VS, Dillard BD, Lanzilotta WN. Substrate-induced conformational changes in *Escherichia coli* taurine/a-ketoglutarate dioxygenase and insight into the oligomeric structure. Biochemistry 2003;42:5547–5554. [PubMed: 12741810]
26. Altschul SF, Madden TL, Schaffer AA, Zhang JH, Zhang Z, Miller W, Lipman DJ. Gapped BLAST and PSI-BLAST: A new generation of protein database search programs. Nucl. Acids Res 1997;25:3389–3402. [PubMed: 9254694]
27. Schäffer AA, Aravind L, Madden TL, Shavirin S, Spouge JL, Wolf YI, Koonin EV, Altschul SF. Improving the accuracy of PSI-BLAST protein database searches with composition-based statistics and other refinements. Nucl. Acids Res 2001;29:2994–3005. [PubMed: 11452024]
28. Ginalski K, Elofsson A, Fisher D, Rychlewski L. 3D-Jury: a simple approach to improve protein structure predictions. Bioinformatics 2003;19:1015–1018. [PubMed: 12761065]
29. Muckstein U, Holfacker IL, Stadler PF. Stochastic pairwise alignments. Bioinformatics 2002;18 (Suppl 2):S153–S160. [PubMed: 12385998]
30. Feig M, Rotkiewicz P, Kolinski A, Skolnick J, Brooks CL III. Accurate reconstruction of all-atom protein representations from side-chain-based low-resolution models. Proteins 2000;41:86–97. [PubMed: 10944396]

31. Feig M, Karanicolas J, Brooks CL III. MMTSB tool set: enhanced sampling and multiscale modeling methods for applications in structural biology. J. Molec. Graphics Modeling 2004;22:377–395.
32. Zhang C, Liu S, Zhu QQ, Zhou YQ. A knowledge-based energy function for protein-ligand, protein-protein, and protein-DNA complexes. J. Med. Chem 2005;48:2325–2335. [PubMed: 15801826]
33. Feig M, Brooks CL III. Evaluating CASP4 predictions with physical energy functions. Proteins: Struct. Funct. Genet 2002;49:232–245. [PubMed: 12211003]
34. Samudrala R, Moult J. An all-atom distance-dependent conditional probability discriminatory function for protein structure prediction. J. Mol. Biol 1998;275:895–916. [PubMed: 9480776]
35. Stumpff-Kane AW, Feig M. A correlation-based method for the enhancement of scoring functions on funnel-shaped energy landscapes. Proteins: Struct., Funct. Bioinform 2006;63:155–164.
36. Ellis KJ, Morrison JF. Buffers of constant ionic strength for studying pH-dependent processes. Meth. Enzymol 1982;87:405–426. [PubMed: 7176924]
37. Counts DF, Cardinale GJ, Udenfriend S. Prolyl hydroxylase half reaction: peptidyl prolyl-independent decarboxylation of a-ketoglutarate. Proc. Natl. Acad. Sci. USA 1978;75:2145–2149. [PubMed: 209453]
38. Rao NV, Adams E. Partial reaction of prolyl hydroxylase. $(Gly\text{-}Gly\text{-}Pro)_n$ stimulates a-ketoglutarate decarboxylation without prolyl hydroxylase. J. Biol. Chem 1978;253:6327–6330. [PubMed: 210178]
39. Holme E, Lindstedt S. Studies on the partial reaction of thymine 7-hydroxylase in the presence of 5-fluorouracil. Biochim. Biophys. Acta 1982;704:278–283. [PubMed: 6213271]
40. Myllylä R, Majamaa K, Günzler V, Hanauske-Abel HN, Kivirikko KI. Ascorbate is consumed stoichiometrically in the uncoupled reactions catalyzed by prolyl 4-hydroxylase and lysyl hydroxylase. J. Biol. Chem 1984;259:5403–5405. [PubMed: 6325436]
41. Kalliri E, Grzyska PK, Hausinger RP. Kinetic and spectroscopic investigation of Co^{II}, Ni^{II}, and *N*-oxalylglycine inhibition of the Fe^{II}/a-ketoglutarate dioxygenase, TauD. Biochem. Biophys. Res. Commun 2005;338:191–197. [PubMed: 16165092]
42. Baader E, Tschank G, Baringhaus KH, Burghard H, Gunzler V. Inhibition of prolyl 4-hydroxylase by oxalyl amino acid derivatives in vitro, in isolated microsomes and in embryonic chicken tissues. Biochem. J 1994;300:525–530. [PubMed: 8002959]
43. Cunliffe CJ, Franklin TJ, Hales NJ, Hill GB. Novel inhibitors of prolyl 4-hydroxylase. 3 Inhibition by the substrate analogue N-oxaloglycine and its derivatives. J. Med. Chem 1992;35:2652–2658. [PubMed: 1321909]
44. Chan DA, Sutphin PD, Denko NC, Giaccia AJ. Role of prolyl hydroxylation in oncogenically stabilized hypoxia-inducible factor-1a. J. Biol. Chem 2002;277:40112–40117. [PubMed: 12186875]
45. McDonough MA, McNeill LA, Tilliet M, Papmichaël CA, Chen Q-Y, Banerji B, Hewitson KS, Schofield CJ. Selective inhibition of factor inhibiting hypoxia-inducible factor. J. Am. Chem. Soc 2005;127:7680–7681. [PubMed: 15913349]
46. Elkins JM, Ryle MJ, Clifton IJ, Dunning-Hotopp JC, Lloyd JS, Burzlaff NI, Baldwin JE, Hausinger RP, Roach PL. X-ray crystal structure of *Escherichia coli* taurine/a-ketoglutarate dioxygenase complexed to ferrous iron and substrates. Biochemistry 2002;41:5185–5192. [PubMed: 11955067]
47. Tramontano A, Morea V. Assessment of homology-based predictions in CASP5. Proteins: Struct. Funct. Genet 2003;53:352–368. [PubMed: 14579324]
48. Kryshtafovych A, Venclovas C, Fidelis K, Moult J. Progress over the first decade of CASP experiments. Proteins: Struct. Funct. Genet 2005;S7:225–236. [PubMed: 16187365]
49. Clifton IJ, McDonough MA, Ehrismann D, Kershaw NJ, Granatino N, Schofield CJ. Structural studies on 2-oxoglutarate oxygenases and related double-stranded b-helix fold protein. J. Inorg. Biochem 2006;100:644–669. [PubMed: 16513174]
50. Muller M, Moller KM. Urate oxidase and its association with peroxisomes in Acanthamoeba sp. Eur. J. Biochem 1969;9
51. Leighton F, Poole B, Lazarow PB, de Duve C. The synthesis and turnover of rat liver peroxisomes. I. Fractionation of peroxisome proteins. J. Cell. Biochem 1969;41:521–535.
52. Nguyen T, Zelechowska M, Foster V, Bergmann H, Verma DPS. Primary structure of the soybean nodulin-35 gene encoding uricase II localized in the peroxisomes of uninfected cells of nodules. Proc. Natl. Acad. Sci. USA 1985;82:5040–5044. [PubMed: 16593585]

53. Breidenbach RW, Kahn A, Beevers H. Characterization of glyoxysomes from castor bean endosperm. Plant Physiol 1968;43:705–713. [PubMed: 16656830]
54. de Hoop MJ, Ab G. Import of proteins into peroxisomes and other microbodies. Biochem. J 1992;286:657–669. [PubMed: 1417723]
55. Petriv OI, Tang L, Titorenko VI, Rachubinski RA. A new definition for the consensus sequence of the peroxisome targeting signal type 2. J. Mol. Biol 2004;341:119–134. [PubMed: 15312767]
56. Reumann S. Specification of the peroxisome targeting signals type 1 and type 2 of plant peroxisomes by bioinformatics analyses. Plant Physiol 2004;135:783–800. [PubMed: 15208424]
57. Swinkels BW, Gould SJ, Bodnar AG, Rachubinski RA, Subramaniam S. A novel, cleavable peroxisomal targeting signal at the amino-terminus of rat 3-ketoacyl-CoA thiolase. EMBO J 1991;10:3255–3262. [PubMed: 1680677]
58. Lee JG, Lee YJ, Lee CH, Maeng PJ. Mutational and functional analysis of the cryptic N-terminal targeting signal for both mitochondria and peroxisomes in yeast peroxisomal citrate synthase. Biochem (Tokyo) 2006;140:121–133.
59. Kato A, Hayashi M, Kondo M, Nishimura M. Transport of peroxisomal proteins synthesized as large precursors in plants. Cell Biochem. Biophys 2000;32:269–275. [PubMed: 11330056]
60. Julenius K, Molgaard A, Gupta R, Brunak S. Prediction, conservation analysis and structural characterization of mammalian mucin-type O-glycosylation sites. Glycobiology 2005;15:153–164. [PubMed: 15385431]
61. Blom N, Gammeltoft S, Brunak S. Sequence- and structure-based prediction of eukaryotic protein phosphorylation sites. J. Mol. Biol 1999;295:1351–1362. [PubMed: 10600390]
62. Cortay J-C, Rieul C, Duclos B, Cozzone AJ. Characterization of the phosphoproteins of *Escherichia coli* cells by electrophoretic analysis. Eur. J. Biochem 1986;159:227–237. [PubMed: 3530754]
63. Ryle MJ, Padmakumar R, Hausinger RP. Stopped-flow kinetic analysis of *Escherichia coli* taurine/a-ketoglutarate dioxygenase: interactions with a-ketoglutarate, taurine, and oxygen. Biochemistry 1999;38:15278–15286. [PubMed: 10563813]
64. Fukumori F, Hausinger RP. Purification and characterization of 2,4-dichlorophenoxyacetate/a-ketoglutarate dioxygenase. J. Biol. Chem 1993;268:24311–24317. [PubMed: 8226980]
65. Mishina Y, Chen LX, He C. Preparation and characterization of the native iron(III)-containing DNA repair AlkB protein directly from *Escherichia coli*. J. Am. Chem. Soc 2004;126:16930–16936. [PubMed: 15612731]
66. Vaillancourt FH, Yin J, Walsh CT. SyrB2 in syringomycin E biosynthesis is a nonheme Fe^{II} a-ketoglutarate- and O_2-dependent halogenase. Proc. Natl. Acad. Sci. USA 2005;102:10111–10116. [PubMed: 16002467]
67. Price JC, Barr EW, Glass TE, Krebs C, Bollinger JM Jr. Evidence for hydrogen abstraction from C1 of taurine by the high-spin Fe(IV) intermediate detected during oxygen activation by taurine:a-ketoglutarate dioxygenase (TauD). J. Am. Chem. Soc 2003;125:13008–13009. [PubMed: 14570457]
68. Hoffart LM, Barr EW, Guyer RB, Bollinger JM Jr. Krebs C. Direct spectroscopic detection of a C-H-cleaving high-spin Fe(IV) complex in a prolyl-4-hydroxylase. Proc. Natl. Acad. Sci. USA 2006;103:14738–14743. [PubMed: 17003127]
69. Busby RW, Chang MD-T, Busby RC, Wimp J, Townsend CA. Expression and purification of two isozymes of clavaminate synthase and initial characterization of the iron binding site. General error analysis in polymerase chain reaction amplification. J. Biol. Chem 1995;270:4262–4269. [PubMed: 7876185]
70. Hegg EL, Whiting AK, Saari RE, McCracken J, Hausinger RP, Que L Jr. Herbicide-degrading a-keto acid-dependent enzyme TfdA: metal coordination environment and mechanistic insights. Biochemistry 1999;38:16714–16726. [PubMed: 10600135]
71. Müller TA, Fleischmann T, van der Meer JR, Kohler H-PE. Purification and characterization of two enantioselective a-ketoglutarate-dependent dioxygenases, RdpA and SdpA, from *Sphingomonas herbicidovorans* MH. Appl. Environ. Microbiol 2006;72:4853–4861. [PubMed: 16820480]
72. Kahnert A, Kertesz MA. Characterization of a sulfur-regulated oxygenative alkylsulfatase from *Pseudomonas putida* S-313. J. Biol. Chem 2000;275:31661–31667. [PubMed: 10913158]
73. Elion GB, Kovensky A, Hitchings GH. Metabolic studies of allopurinol, an inhibitor of xanthine oxidase. Biochem. Pharmacol 1966;15:863–880. [PubMed: 5967902]

74. Edmondson D, Ballou DP, Vn Heuvelen A, Palmer G, Massey V. Kinetic studies on the substrate reduction of xanthine oxidase. J. Biol. Chem 1973;248:6135–6144. [PubMed: 4353632]

75. McWhirter RB, Hille R. The reductive half-reaction of xanthine oxidase. Identification of spectral intermediates in the hydroxylation of 2-hydroxy-6-methylpurine. J. Biol. Chem 1991;266:23724–23731. [PubMed: 1660883]

76. Ivan M, Kondo K, Yang H, Kim W, Valiando J, Ohh M, Salic A, Asara JM, Lane WS, Kaelin WG Jr. HIFa targeted for VHL-mediated destruction by proline hydroxylation: implications for O_2 sensing. Science 2001;292:464–467. [PubMed: 11292862]

77. Jaakkola P, Mole DR, Tian Y-M, Wilson MI, Gielbert J, Gaskell SJ, von Kriegsheim A, Hebestreit HF, Mukherji M, Schofield CJ, Maxwell PH, Pugh CW, Ratcliffe PJ. Targeting of HIF-a to the von Hippel-Lindau ubiquitylation complex by O_2-regulated prolyl hydroxylation. Science 2001;292:468–472. [PubMed: 11292861]

78. Hogan DA, Auchtung TA, Hausinger RP. Cloning and characterization of a sulfonate/a-ketoglutarate dioxygenase from *Saccharomyces cerevisiae*. J. Bacteriol 1999;181:5876–5879. [PubMed: 10482536]

79. Okamoto K, Matsumoto K, Hille R, Eger BT, Pai EF, Nishino T. The crystal structure of xanthine oxidoreductase during catalysis: implications for reaction mechanism and enzyme inhibition. Proc. Natl. Acad. Sci. USA 2004;101:7931–7936. [PubMed: 15148401]

80. Retailleau P, Colloc'h N, Vivarés D, Bonneté F, Castro B, El Hajji M, Mornon J-P, Monard g. Prangé T. Complexed and ligand-free high-resolution structures of urate oxidase (Uox) from Aspergillus flavus: a reassignment of the active-site binding mode. Acta Crystallogr 2004;D60:453–462.

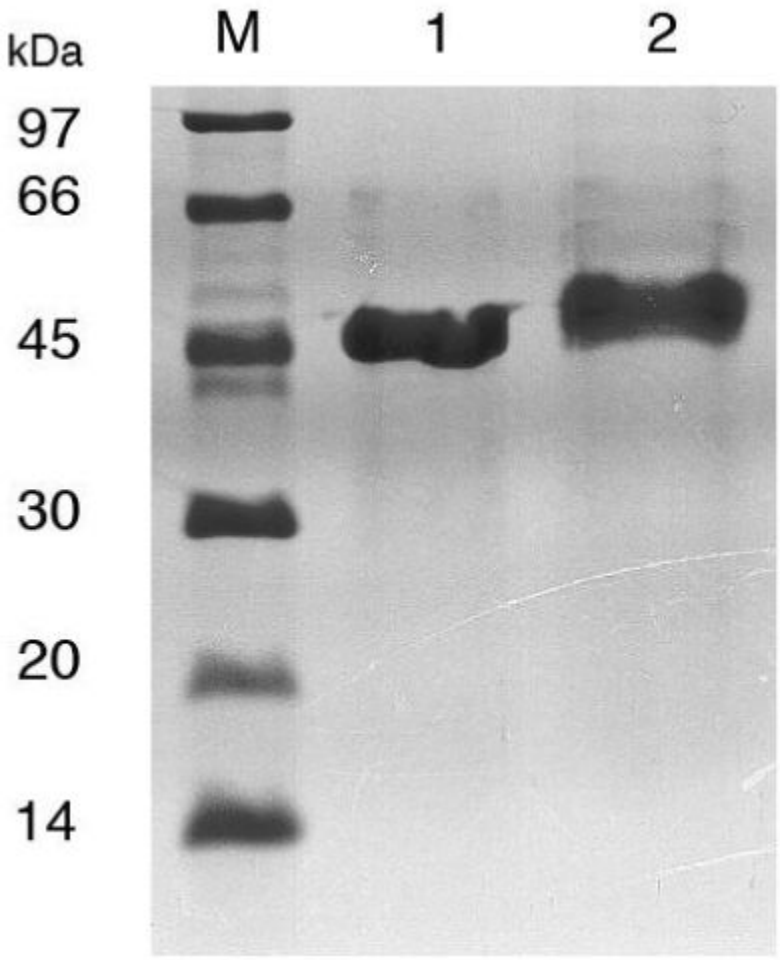

FIGURE 1.
SDS-PAGE analysis of the purified XanA from *E. coli* and *A. nidulans*. Comparison of the purified XanA protein derived from *A. nidulans* and *E. coli*. Lane M, markers; lane 1, sample purified from the fungus; lane 2, protein isolated from the bacterium (7 μg each). Stacking and running gels contain 5 % and 12 % acrylamide.

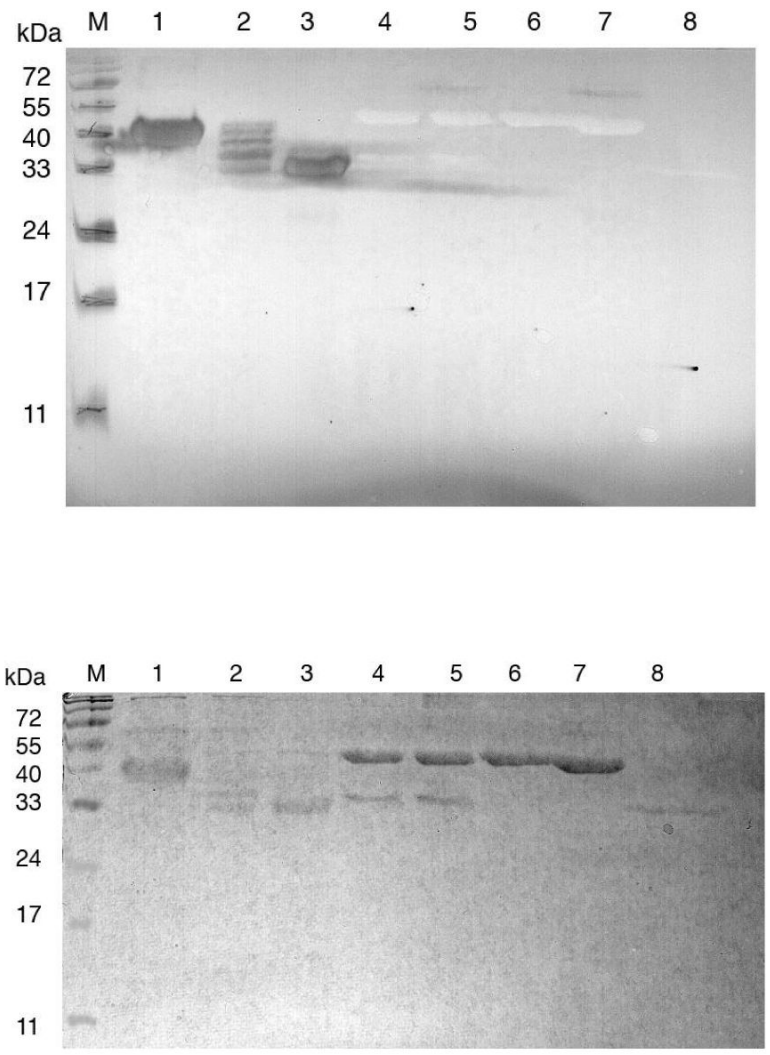

FIGURE 2.

Glycosylation analysis of XanA derived from *E. coli* and *A. nidulans*. (Upper panel) Protein-linked carbohydrate was detected in XanA samples (5 μg each) by using an immunoassay (DIG glycan detection kit, Roche). Lane M, protein size markers (Fermentas); lane 1, XanA purified from *A. nidulans*; lane 2, PNGase F-treated native XanA purified from *A. nidulans*; lane 3, PNGase F-treated XanA from *A. nidulans* after denaturation; lane 4, PNGase F-treated native XanA purified from *E. coli*; lane 5, PNGase F-treated XanA from *E. coli* after denaturation; lanes 6 and 7, XanA from *E. coli*; lane 8, PNGase F. (Lower panel) The same samples were stained for protein by Coomassie blue.

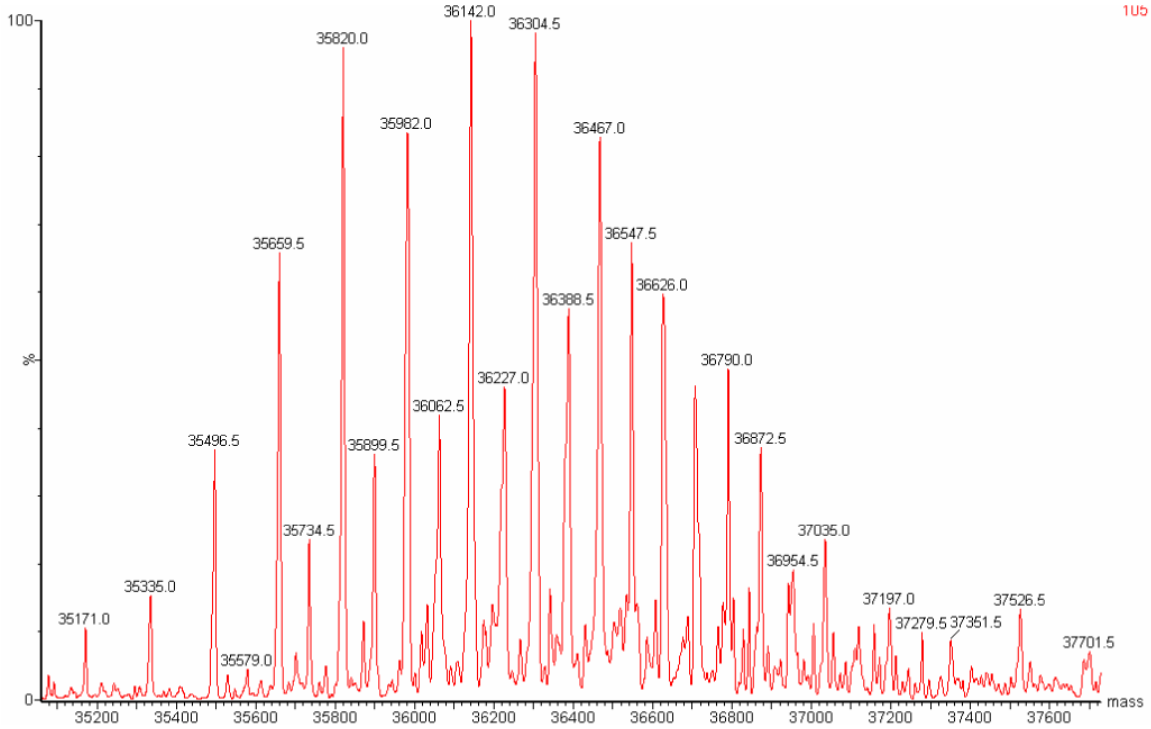

FIGURE 3.

Mass spectrometric analysis of fungus-derived XanA. The XanA protein isolated from *A. nidulans* was analyzed by electrospray ionization mass spectrometry. The figure depicts a series of peaks separated by 162 mass units and 80 mass units, consistent with glycosylation and phosphorylation, respectively.

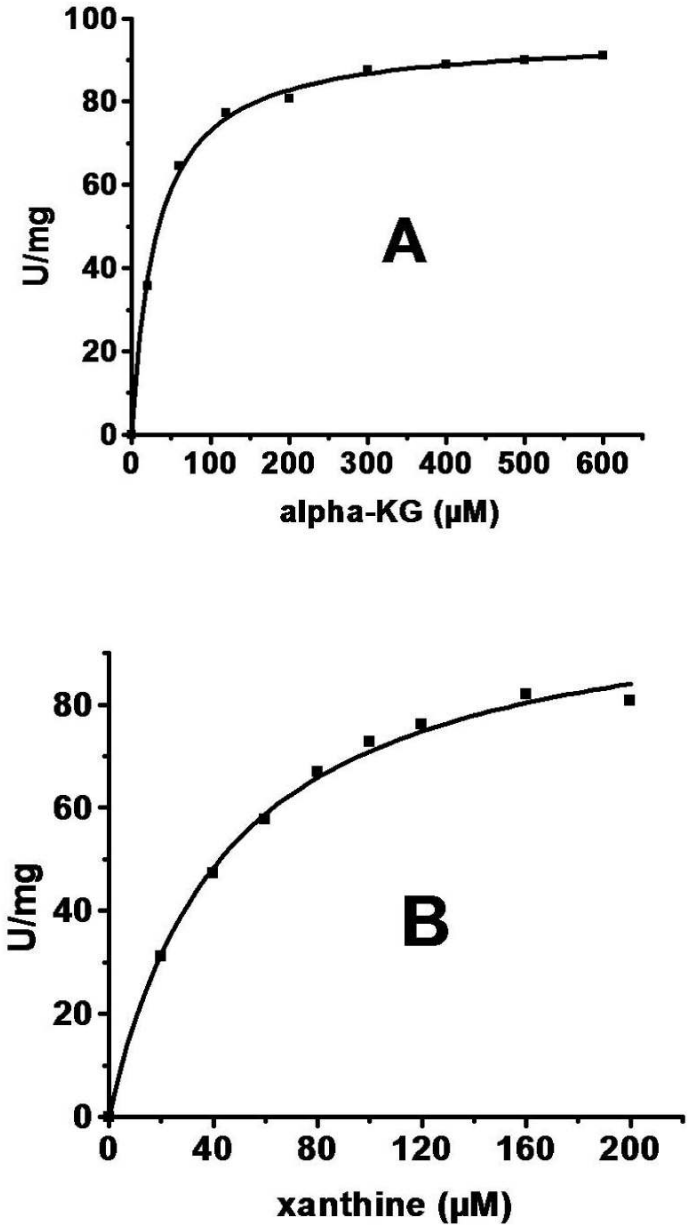

FIGURE 4.

Substrate and co-substrate concentration dependencies of XanA. The effects of varying the concentrations of (A) αKG and (B) xanthine on xanthine/αKG dioxygenase activity were examined for the *E. coli*-derived protein at 25 °C. Except for the compound being varied, the assay solutions contained 40 μM Fe^{II}, 1 mM KG, and 200 μM xanthine in 50 mM MOPS buffer, pH 7.4. The data were fit to the Michaelis-Menten equation.

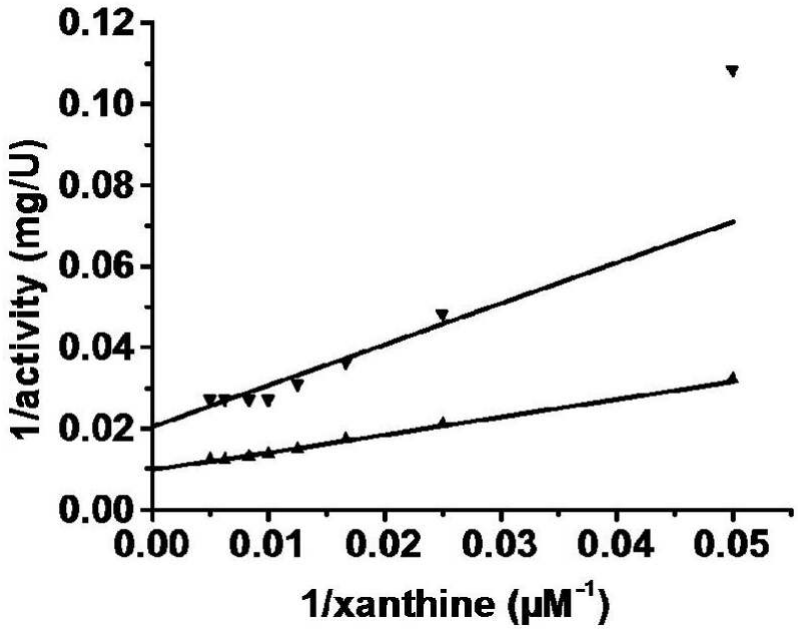

FIGURE 5.

Solvent deuterium isotope effect on XanA activity. The effects of varying the concentration of xanthine on xanthine/αKG dioxygenase activity were examined at 25 °C in 50 mM MOPS buffer, p^2H 8.0 (▼) (p^2H values were determined by adding 0.4 to the pH electrode reading) or pH 7.6 (▲) containing 40 μM Fe^{II}, 1 mM αKG, and 0-200 μM xanthine.

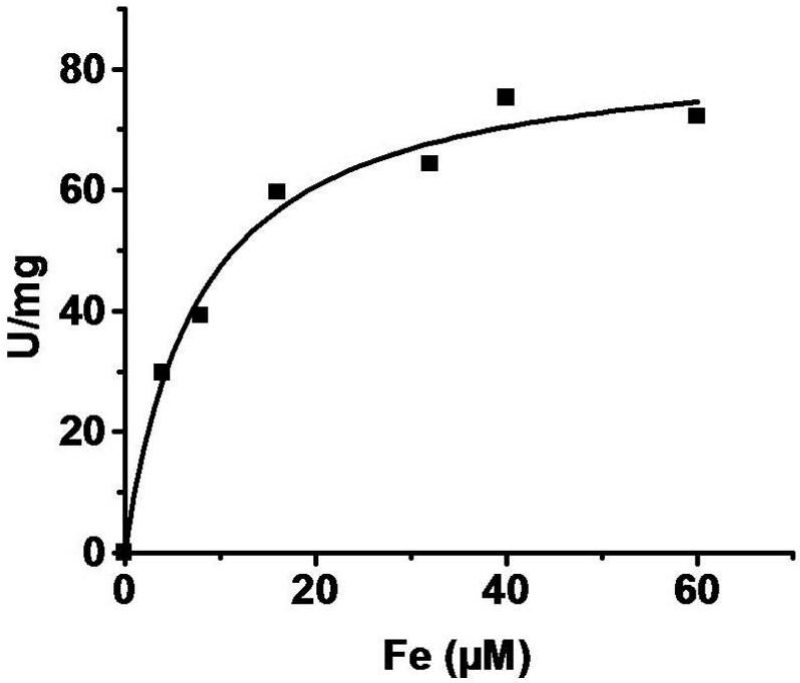

FIGURE 6.

Fe^{II} concentration dependence of XanA. The effects of varying the concentration of Fe^{II} on xanthine/αKG dioxygenase activity were examined by using the *E. coli*-derived protein at 25 °C in solutions containing 1 mM KG and 200 μM xanthine in 50 mM MOPS buffer, pH 7.4.

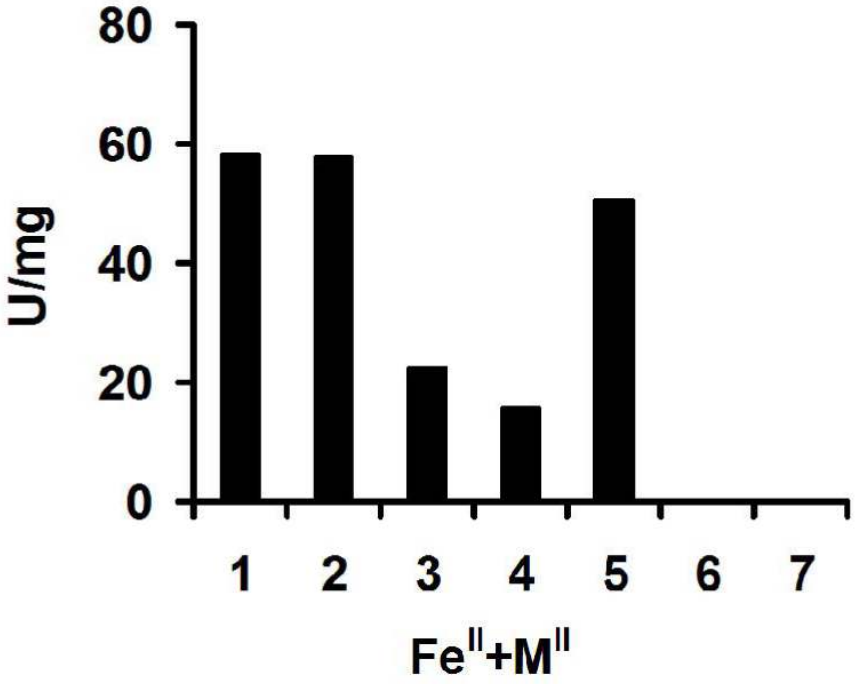

FIGURE 7.

Divalent cation inhibition of XanA. The effects of several divalent cations (M^{II}, at 40 μM concentration) on xanthine/αKG dioxygenase activity were examined by using the *E. coli*-derived protein at 25 °C in solutions containing 40 μM Fe^{II}, 1 mM αKG and 200 μM xanthine in 50 mM MOPS buffer, pH 7.4. Samples included (1) Fe^{II} only and Fe^{II} plus (2) Mg^{II}, (3) Mn^{II}, (4) Co^{II}, (5) Ni^{II}, (6) Zn^{II}, (7) Cu^{II}.

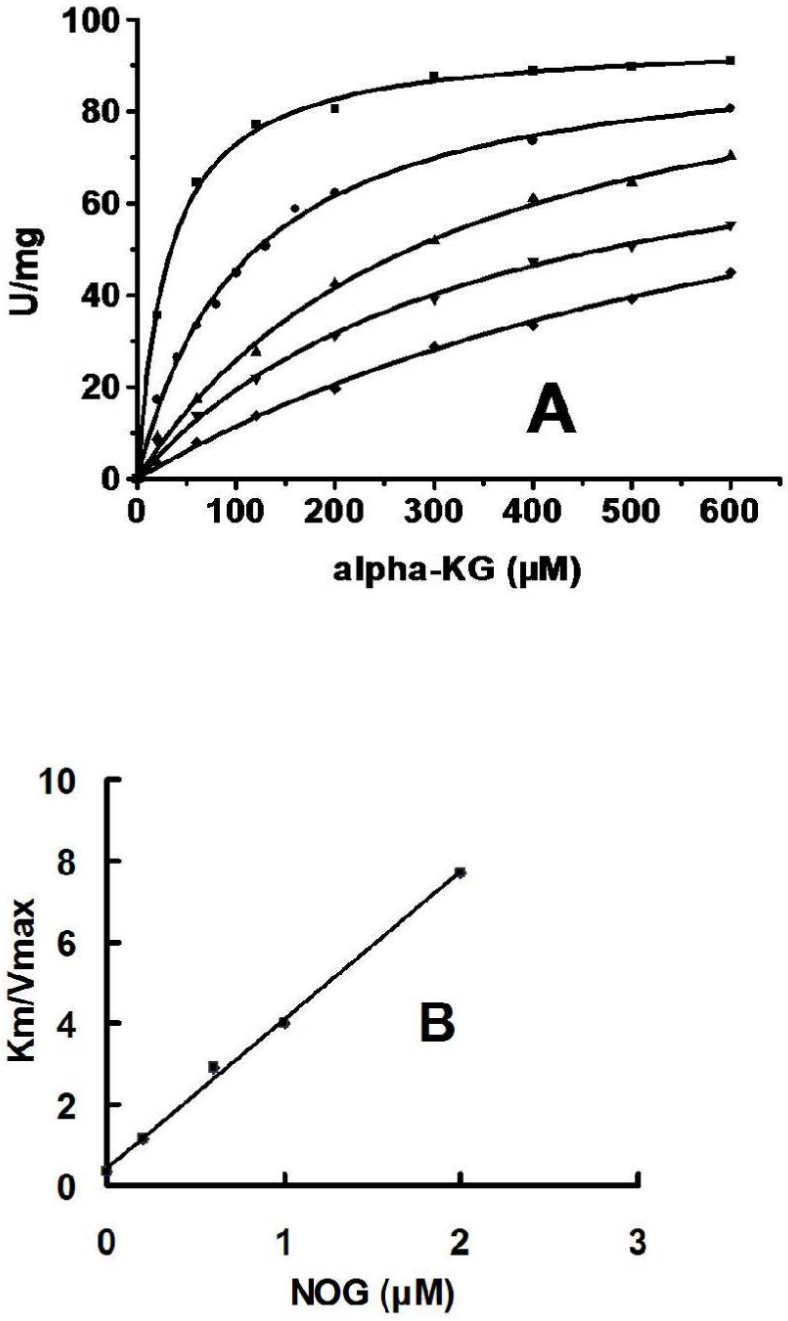

FIGURE 8.

NOG inhibition of XanA. (A) The effects of varying concentrations of NOG (0, 0.2, 0.6, 1.2, and 2 μM) on xanthine/μKG dioxygenase activity were examined by using the *E. coli*-derived protein at 25 °C in solutions containing 40 μM Fe^{II}, 1 mM αKG and 200 μM xanthine in 50 mM MOPS buffer, pH 7.4. Each set of initial rate data was fit to the Michaelis-Menten equation. (B) A replot of the values of apparent K_m divided by apparent V_{max} as a function of inhibitor concentration.

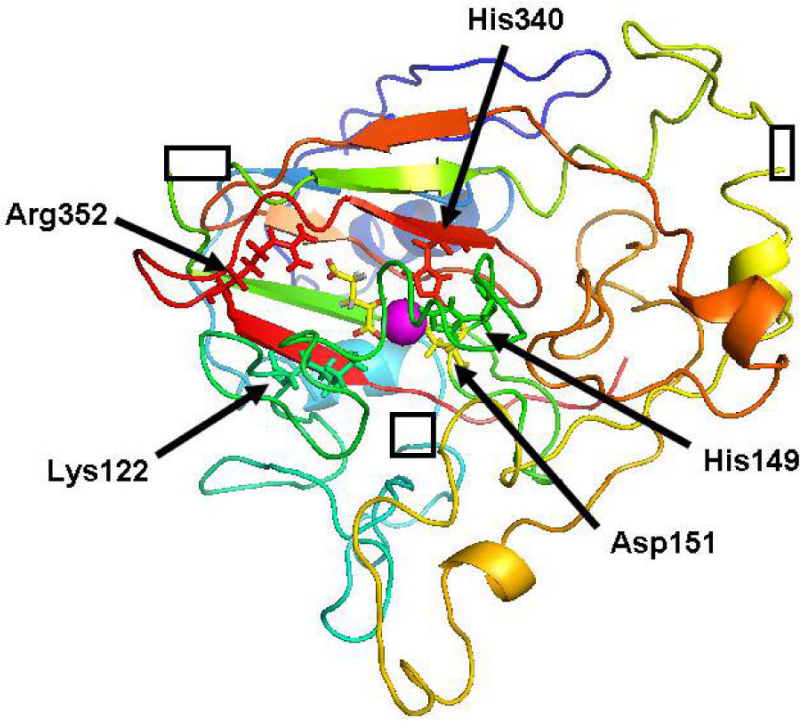

FIGURE 9.

Homology model of XanA. Ribbon diagram depicting the XanA homology model predicted by using TauD (PDB code 1OS7, A chain) as a template. The polypeptide chain is depicted in blue to red coloration (*N*-terminus to *C*-terminus) with gaps indicated by boxes for the non-modeled loops involving residues 72-88, 173-190, and 219-231. The postulated metal ligands (His149, Asp151, and His340) are illustrated in green, yellow, and red, respectively, to the right of the magenta Fe^{II} sphere. Bound KG (yellow) chelates the metals and is suggested to be stabilized by a salt bridge to the C-5 carboxylate involving Arg352 (red) and a hydrogen bond to the C-1 carboxylate via Lys122 (green).

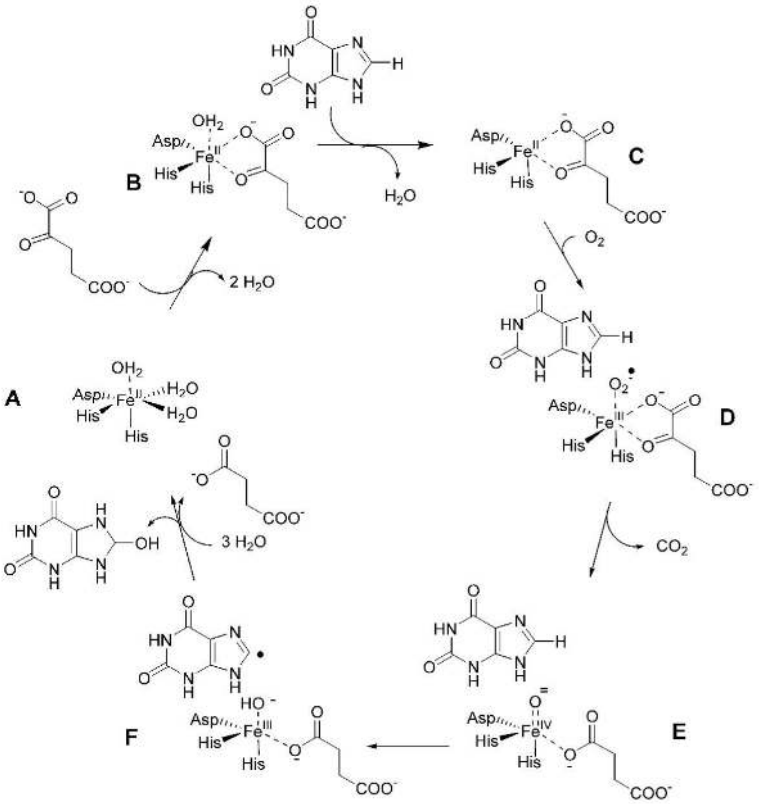

Scheme 1.